

Multi Activity Sequence Alignment via Implicit Clustering

Taein Kwon¹

Zador Pataki¹

Mahdi Rad²

Marc Pollefeys^{1,2}

¹ETH Zürich

²Microsoft MR & AI Lab, Zürich

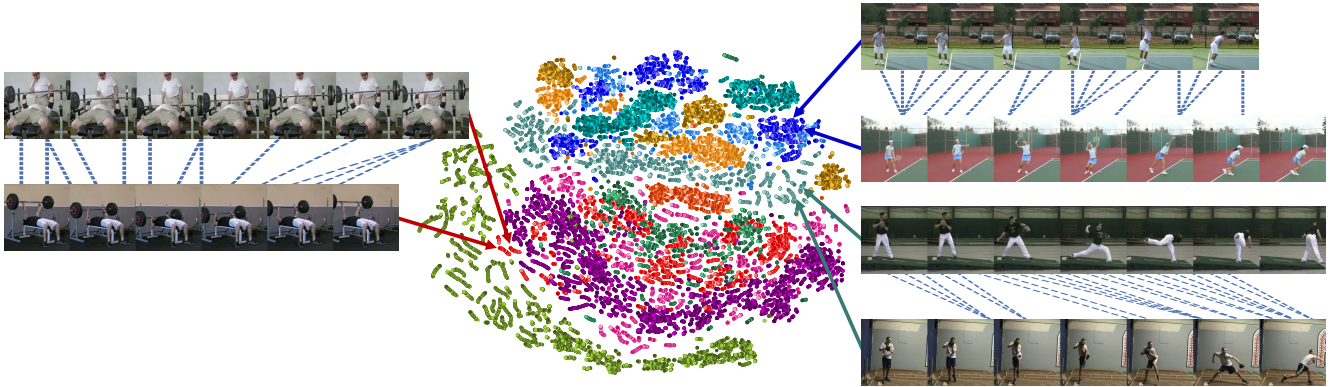


Figure 1. **The t-SNE visualization of the learned embeddings on the PennAction dataset.** The proposed method effectively distinguishes different activities. On the left, the alignment of two bench pressing sequences is shown, which demonstrates the effectiveness of our approach. On the right, our model not only differentiates between activities like baseball pitch and tennis serve but also recognizes their proximity in the embedding domain. Dashed lines indicate matched frames between sequences.

Abstract

Self-supervised temporal sequence alignment can provide rich and effective representations for a wide range of applications. However, existing methods for achieving optimal performance are mostly limited to aligning sequences of the same activity only and require separate models to be trained for each activity. We propose a novel framework that overcomes these limitations using sequence alignment via implicit clustering. Specifically, our key idea is to perform implicit clip-level clustering while aligning frames in sequences. This coupled with our proposed dual augmentation technique enhances the network’s ability to learn generalizable and discriminative representations. Our experiments show that our proposed method outperforms state-of-the-art results and highlight the generalization capability of our framework with multi activity and different modalities on three diverse datasets, H2O, PennAction, and IKEA ASM. We will release our code upon acceptance.

1. Introduction

Dense temporal alignment of videos [16, 37] is a fundamental task in computer vision, which aims to find the optimal frame-wise correspondence between two or more video se-

quences. It has many applications, such as frame retrieval, action recognition, abnormality detection, and skill transfer. Moreover, the advancements in AR and VR have created new opportunities for utilizing temporal alignment in understanding human activity, supported by diverse modalities such as RGB images, hand movements, and body poses.

To learn dense temporal alignment, supervised learning-based methods require large amounts of labeled data for each activity category and alignment. However, manually labeling data is expensive, limiting the generalizability and scalability of these methods to new activities and domains. Hence, there has been a focus on using self-supervised learning methods, such as cycle consistency [16] and temporal alignment [21], to perform dense video alignment. However, when extending these methods to encompass *multiple activities*, they require action labels as their nature are primarily designed for videos of the same activity. Consequently, they either operate solely on single-activity videos or require a separate model to be trained for each activity.

Unlike previous methods, contrastive learning-based methods, on RGB [7, 37] or on appearance-invariant data such as skeletal [28, 42] can be trained on multiple activities without requiring any additional labels. However, as our experiments show, when these methods are trained on multiple activities, the learned embeddings tend to collapse into a single homogeneous space across different activities,

resulting in difficulties in distinguishing between different activities, and therefore limiting the applicability of temporal video alignment in real-world scenarios.

In this paper, we introduce a novel framework for self-supervised sequence alignment that overcomes these limitations by leveraging the power of implicit clustering techniques. We name it MASA (Multi Activity Sequence Alignment). As illustrated in Figure 1, MASA is not only able to learn discriminative representations between different activities but also recognize the proximity of similar activities in the embedding domain. MASA consists of three main components: the augmentation module, the context-aware module, and the alignment-cluster module. The augmentation module applies our augmentation techniques to each sequence to perform contrastive style learning. The context-aware module then extracts embeddings from the input sequences, capturing rich temporal information. Finally, the novel alignment-cluster module performs implicit clustering and matching of frames between input sequences. Inspired by [9], originally designed for image classification tasks, we extend the concept to clip-level clustering by leveraging the attention mechanism, to map each sequence to a latent vector that represents its clustering prototype via the clip-level clustering predictor. In addition to the novel alignment-cluster module, we propose a dual augmentation technique that aids in learning more generalizable and discriminative representations than the existing methods [28, 42]. The existing techniques lack the diversity of temporal variations, whereas ours provides a wider range. By jointly optimizing these modules, MASA can cluster and align sequences in a self-supervised fashion.

We conduct a thorough evaluation of the effectiveness of our approach by assessing its performance in various downstream tasks related to fine-grained video understanding, such as phase classification, phase progress, Kendall tau, and frame retrieval, on three diverse datasets: H2O [27], PennAction [51], and IKEA ASM [3], which contain diverse temporal range from a few seconds to minutes for activities. As light representations of human/hand poses and motions such as 3D skeletons are beneficial for AR and VR scenarios, we show our proposed method can perform well on these representations and it is not limited to RGB images only. Moreover, 3D skeletons can be obtained easily thanks to recent off-the-shelf methods and often from AR and VR devices. Furthermore, we show the clustering ability of the proposed network by performing action recognition across different activities. Our method can leverage multiple modalities, and results in even better accuracy.

Our main contributions are summarized as follows:

- We introduce MASA, a novel framework for multi activity sequence alignment, which can effectively handle a wide range of activities and scenarios.
- We propose implicit clip-level clustering, which identi-

fies prototypes of different activities in the latent space. To the best of our knowledge, we are the first to leverage implicit clustering while optimizing sequence alignment. With our proposed dual augmentation technique, the implicit clip-level clustering enables the framework to learn more generalizable and discriminative representations.

- We demonstrate MASA is not limited to RGB only, and it can perform on different modalities such as skeleton, showing its generalization ability.
- We prove MASA achieves state-of-the-art on most of the metrics on both modalities, RGB and skeleton. Notably, MASA is not only able to handle multiple activities to train on a single model, but it also leverages the diverse activity data to boost overall performance even further. Previous approaches, however, suffer performance degradation with multiple activities on a single model.

We demonstrate the superiority of MASA on three diverse datasets and provide ablation studies and quantitative analysis as well as showing clustering performance through the action recognition task for both RGB and skeleton inputs.

2. Related Work

Self-Supervised Representation Learning. Driven by the need to scale up training by leveraging unlabeled data, self-supervised learning (SSL) has become a crucial method in vision analysis. Pioneering works explored contrastive learning approaches to learn image representations in a self-supervised manner. SimCLR [8] demonstrated the benefits of data augmentation and contrasting representations in a remapped latent space, while [46] and MoCo [10, 22] identified performance improvements resulting from a large number of negative anchors. Recent works explored the benefits of combining clustering and representation learning [2, 4, 9], and BYOL [19] and SimSiam [9] introduced implicit clustering with contrastive learning approaches that do not rely on negative samples. Besides contrastive learning, MAE [23] and DINO [5] learn effective image representations using masked autoencoding and self-distillation respectively. Contrastive learning approaches have also been extended to learn video-level representations [13, 18, 24, 35]. Inspired by the field of Natural Language Processing, future frame prediction has been explored [1, 14] and MAE inspired a series of works in video-level representation learning [41, 44]. In this work, we explore the pretext task of sequence alignment as an SSL approach for clip-level representation learning. Furthermore, we demonstrate that employing clip-level implicit clustering can generalize to multi activity sequence alignment.

Sequence Alignment. Sequence alignment in video analysis refers to the process of aligning sequences of frames or actions across different videos. Early methods, such as TCN [37], utilized contrastive learning on synchronized

frames across views. This method, however, lacks scalability due to the need for a multi-camera setup. TCC [16] introduced scalable SSL through temporal cycle-consistency for robust frame correspondence. Subsequent developments like LAV [21] and VAVA [31] adopted dynamic time warping and optimal transport for SSL in video alignment. These methods, however, require action labels when they train all activities in one model. Alternatively, CARL [7] extracts random clips from a video, while VSP [50] employs stochastic process modeling to enable contrastive learning. For skeleton features, CASA [28], using sequence augmentation and transformer-based attention, significantly improved frame-wise embeddings for 3D skeletons, with LA2DS [42] following suit. However, these augmentation-based methods [7, 28, 42], stochastic modeling method [49] are not dedicatedly designed for multi activity scenarios and often face limitations in action-specific generalization. More recently, GTCC [15] employs the Gaussian mixture model and context-dependent drop function to generalize TCC [16]. However, their performance is suboptimal compared to other methods [7, 31]. MASA overcomes this by employing implicit clustering to train networks capable of generating action-generalizable embeddings as well as distinguishing across different activities.

Action Recognition. Action recognition is a task in computer vision that involves identifying and classifying human actions based on a sequence of data. While supervised methods [6, 17] were widely used before, with the development of large-scale video datasets, video representation learning [20, 34, 35, 41, 44], which treats action recognition as downstream tasks, has gained popularity. In AR and VR scenarios, skeletal action recognition has drawn significant attention [11, 12, 30, 32, 38, 45, 48] due to its light representation, especially as mixed reality devices often provide skeletons prediction. Similar to video representation learning with RGB data, recent advancements in skeletal action recognition have explored SSL methods, including contrastive learning [40] and using future pose prediction as a pretext task [29]. Furthermore, clustering has helped improve representation qualities [26, 39], and node-level MAE has been deployed in skeleton sequences [33, 47]. We demonstrate the effectiveness of our SSL sequence representation on multi activity by implicit clustering in action recognition benchmarks.

3. Method

We present the details of our proposed framework for self-supervised sequence alignment as shown in Figure 2. MASA consists of three main components: the augmentation module, which performs dual augmentation for the given sequence at training time, the context-aware module which extracts embedding from the input sequences, and

the alignment-cluster module which implicitly clusters and matches the frames between the input sequences.

3.1. Dual Augmentation

Existing methods [28, 42] use a temporal augmentation technique such that given a sequence, they generate one augmented sequence for alignment by randomly dropping a number of frames. However, this is suboptimal as it limits the models to learn alignment sequences with faster speed only. We, therefore, propose to extend this technique to Dual Augmentation. Our technique aims to generate two different augmented sequences $\mathcal{S}' = \{s'_j\}^M$ and $\mathcal{S}'' = \{s''_k\}^N$ from the same original sequence \mathcal{S} with the random trimming length M and N , where s'_j and s''_k are individual frames of the corresponding sequences. We then randomly trim the original sequence and apply individual temporal augmentation for each sequence, \mathcal{S}' and \mathcal{S}'' , ensuring that the sequence range remains consistent during clustering. In addition to the advantage of supporting both faster and slower sequences, dual augmentation increases the diversity and complexity of the input sequences, which can help the network learn more generalizable and discriminative representations. This, however, requires a novel matching loss function, which we will present in Section 3.3. Moreover, the random trimming technique, while augmenting the sequence, helps to learn partially trimmed sequence clustering without knowing the entire sequence information, leading to a better clustering performance together with the clustering predictor. Furthermore, dual augmentation allows the network to handle cases where some frames from the original sequence are not present in either of the augmented sequences, which can happen due to random dropping. This can enhance the network’s ability to recover missing information and fill in the gaps. Therefore, while augmenting, we compute $g'(\cdot)$ and $g''(\cdot)$, which map indices from \mathcal{S}' and \mathcal{S}'' to their original index in \mathcal{S} , respectively. Note that we only perform this trim augmentation for RGB images because the 3D skeleton representation is already compact, and additional trimming results in less context information.

In practice, for spatial augmentation, we follow the augmentation techniques proposed in [42] such as angle, flip, translation and VPoser augmentations. For RGB augmentation, we only perform dual augmentation temporally. We provide a detailed explanation of these techniques in the supplementary material.

3.2. Context-Aware Module

The context-aware module aims to extract the embeddings from the input sequences that capture the temporal information of the frames. The input sequences are obtained by applying two different augmentations to the original video sequence. The module first extracts a feature representa-

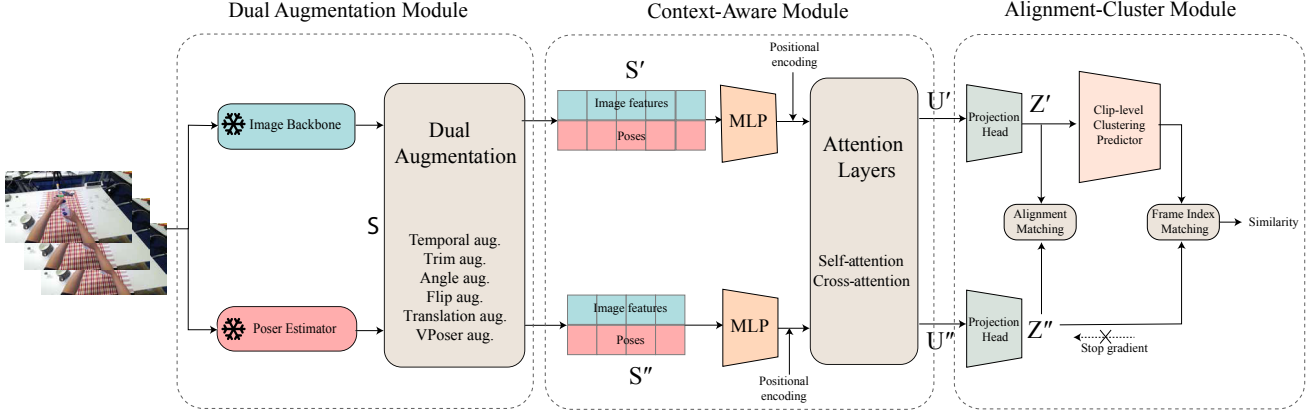


Figure 2. **System Overview.** Our framework takes RGB images as inputs and obtains RGB features using the frozen DINO [34] pre-trained model and skeletons extracted using FrankMocap [36]. Dual augmentation generates two different augmented sequences with frame-wise concatenated image features and skeletons. Note that when we use only one modality, we disable the other modality and feed it to the context-aware module without concatenation. Our context-aware module extracts embeddings for the downstream tasks. The alignment module matches and clusters the latent features to learn framewise video embeddings.

tion of each frame using an MLP model and then employs temporal positional encoding to embed temporal context. We employ sine and cosine function-based positional encoding by following the success of the Transformer [43]. We then pass this information to the encoder, which consists of self- and cross-attention encoders. Self-attention layers learn about the relation between frames within the same sequence, while cross-attention layers learn the relation between frames across augmented sequences. The output of the context-aware module is a set of embeddings that encode both the spatial and temporal information of the input sequences as follows:

$$(U', U'') = A(f(S') + PE_{S'}, f(S'') + PE_{S''}), \quad (1)$$

where $f(\cdot)$ is the MLP model described above, PE is the positional encoding, and $A(\cdot)$ is the attention-based encoder.

3.3. Alignment-Cluster Module

The alignment module aims to find the optimal temporal alignment between the input sequences. It takes the embeddings from the context-aware module as inputs and matches them framewise to learn alignment between two augmented sequences. In practice, we first employ Projection head to the embeddings computed by the context-aware module, which is suggested by SimCLR [8]. This head prevents the embedding space from overfitting to the target tasks, such as frame alignment and clustering, and makes the representation perform downstream tasks easier.

Matching. The matching algorithm is a key component of the alignment module. It learns to align two augmented sequences by minimizing the distance between their indices with respect to the original sequence, in a regression-based

fashion. MASA is designed in bi-direction unlike the previous methods [28, 42], which only consider uni-direction to calculate distance, thanks to the dual augmentation.

More specifically, let Z' and Z'' be the output of the projection head $P(\cdot)$ given the computed embeddings of the sequences U' and U'' , respectively. Following [16, 28, 42], we then calculate $\gamma_{j,k}$ the probability of a frame index j , where frame $s'_j \in S'$, being a match, to frame index k , where $s''_k \in S''$, as

$$\gamma_{j,k} = \frac{\exp(\mathcal{D}(Z'_j, Z''_k))}{\sum_{n=1}^N \exp(\mathcal{D}(Z'_j, Z''_n))}, \quad (2)$$

where $\mathcal{D}(\cdot)$ is the cosine similarity function, N is number of frames in the augmented sequence S'' . While [28] uses distance instead of cosine similarity, in our experiments, cosine similarity resulted in a faster and more stabilized convergence during training.

We then predict the frame index, \hat{j} , in the original sequence S , by weighing the frame indices with their corresponding probabilities, as follows:

$$\hat{j} = \sum_{k=1}^N (\gamma_{j,k} \cdot g''(k)). \quad (3)$$

The loss $\mathcal{L}_{S' \rightarrow S''}$ can be computed as the mean squared error between the predicted frame index \hat{j} and its ground truth frame index, which is preserved after augmentation:

$$\mathcal{L}_{S' \rightarrow S''} = \frac{1}{M} \sum_{j=1}^M |g'(j) - \hat{j}|, \quad (4)$$

To have a symmetrized loss we can similarly compute the $\mathcal{L}_{S'' \rightarrow S'}$ as:

$$\mathcal{L}_{S'' \mapsto S'} = \frac{1}{N} \sum_{k=1}^N \left| g''(k) - \hat{k} \right|, \quad (5)$$

where \hat{k} is the predicted frame index of frame k in the original sequence S'' , where $s_k'' \in S''$, and M is the number of frames in the augmented sequence S' . The final matching loss then can be defined as follows:

$$\mathcal{L}_m = \frac{1}{2} (\mathcal{L}_{S' \mapsto S''} + \mathcal{L}_{S'' \mapsto S'}). \quad (6)$$

Clip-level Implicit Clustering. Our implicit clustering component is inspired by [9], which introduces representation learning using a Siamese network architecture with image clustering. One side of the Siamese network is extended by introducing a clustering predictor, and a stop-gradient operation is applied on the other side. Simsim [9], however, is designed to work on a single image only and does not perform on videos. We, therefore, extend its concept to clip-level clustering instead of frame-level clustering, by composing attention layers and a matching method to the clustering predictor for better frame alignment and action classification, unlike the original Simsim [9]. This helps to capture temporal context and leverage it in the domain for sequence alignment.

The clip-level clustering predictor H learns to map each output of the projection head Z' or Z'' to a latent space, which represents its clustering prototype by maximizing the similarity between both latent vectors. At the same time, stop-gradient, which prevents gradient descent flow from the other latent vector of the clustering predictor, plays an essential role in preventing collapsing as the optimizer quickly finds a degenerated solution, and encourages the network to learn diverse and invariant features [9]. Our ablation study shows the impact of the stop gradient for the task of temporal sequence alignment. Similar to the matching loss, we also define a symmetrized loss as:

$$\mathcal{L}_c = \frac{1}{2} (\mathcal{F}(\text{stopgrad}(Z'), H(Z'')) + \mathcal{F}(\text{stopgrad}(Z''), H(Z'))) \quad (7)$$

where $\text{stopgrad}(\cdot)$ is the stop-gradient operation that prevents the gradient from being propagated from Z' and Z'' in the first and second terms, respectively.

After passing through H , the embeddings keep the temporal dimensionality and match between the clustering predictor and input sequence by matching function $\mathcal{F}(\cdot)$, which preserves temporal information, enabling H to predict clip-level prototype activities effectively. $\mathcal{F}(\cdot)$ calculates the negative cosine similarity based on matching indices in the original sequence as

$$\mathcal{F}(\cdot | g', g'')(V, W) = \sum_{j=0}^M \sum_{k=0}^N \delta_{g'(j), g''(k)} \mathcal{D}(V_j, W_k), \quad (8)$$

where $\delta_{x,y}$ is Kronecker delta function, which is 1 if $x = y$ and 0 otherwise.

Taking into account the disparity in the range of \mathcal{L}_m and \mathcal{L}_c , we optimize the following loss over the parameters of the networks as

$$\mathcal{L} = \mathcal{L}_m \cdot \frac{2}{(1 + \epsilon) + \mathcal{L}_c}. \quad (9)$$

\mathcal{L}_c varies between -1 and $+1$, we therefore add ϵ (in practice we use $\epsilon = 1 \times 10^{-7}$) to the denominator to ensure preventing division by zero. While L_c prevents the latent space from collapsing across different activities, L_m contributes to the sequence alignment, allowing the model to capture similarities between activities.

At the inference, we feed the sequences without augmentation and utilize embeddings \mathcal{U}' to evaluate our model.

4. Evaluation

In this section, we present and discuss the results of our evaluation on three datasets. We first describe the datasets and the implementation details. Then, we describe the evaluation metrics used in this paper. We then show the performance of the proposed method on the tasks of Fine-grained Video Understanding and Action Recognition and compare it to the state-of-the-art methods. Finally, we demonstrate the results of an ablative analysis of our method.

4.1. Datasets

We evaluate our performance on three different datasets, PennAction [51], IKEA ASM [3], and H2O [27] following [28, 42].

H2O. The H2O dataset collects 3D hand poses and object poses while subjects perform a series of actions with a multi-view and an egocentric view. CASA [28] selects the monotonic videos from one activity, Pouring Milk, and annotates the phases accordingly. The Pouring Milk activity contains 38 sequences, 10 phases. The longest sequence has a maximum of 865 frames. The entire dataset has 36 actions, 184 videos, and the longest sequence has a maximum of 1238 frames. 3D hand poses are provided in this dataset, therefore, similar to [28] we use these poses as the source of input sequences.

PennAction. The PennAction dataset is a collection of sports activities. For training and evaluation, we use the same 13 subset actions as [16, 21, 28, 31, 42]. These subset actions are divided into 2 to 6 phases, 371 videos, and up to

663 frames. To obtain the body poses for this dataset, we use FrankMocap [36].

IKEA ASM. The IKEA ASM dataset captures human activity during furniture assembly. Following [21, 28, 31, 42], we train and evaluate on the Kallax Drawer Shelf sequences. They are divided into 17 phases and contain 90 videos up to 4078 frames. We obtain the body poses similar to the PennAction dataset.

4.2. Implementation Details

Model Architecture. The model consists of the following network components: a multilayer perceptron (MLP), a self- and cross-attention module, a projection head, and a cluster predictor. The model aims to learn temporal context and alignment between augmented sequences.

MLP. We use a multilayer perceptron model (MLP) to transform the features from different modalities and align them to the same dimensionality. The MLP consists of three fully connected layers with ReLU activation. The input, hidden, and output layers are 1536, 512, and 128 for RGB modality, and have the same dimension as the input stream for 3D skeletons. For RGB modality, we use a pretrained network DINO [34] to extract features from the RGB images, and then pass them to the MLP to obtain the features in the same dimension as the corresponding dataset. For 3D skeleton modality, we use the hand keypoints for the H2O dataset $s_{\text{H2O}} \in \mathbb{R}^{17 \times 2 \times 3}$ and body keypoints $s_{\text{PennAction}} \in \mathbb{R}^{25 \times 3}$ and $s_{\text{IKEA ASM}} \in \mathbb{R}^{25 \times 3}$ for PennAction and IKEA ASM, respectively. The MLP allows us to extract and reorder the features to fit into the network architecture and enhance the performance. As we use MLP, we set the length of the input as the maximum frame length of the dataset and perform zero-padding where the length is longer than the input sequence.

Self- and Cross-Attention. We have self- /cross-attention encoders as our encoder of the network. We set the 4 attention layers alternately to maximize temporal context learning capability. The keys and values are target features, and the queries are source features in the cross-attention layer.

Projection Head. We set 4 fully connected layers for Projection head. Different from CASA [28], we also incorporate batch-normalization inspired by SimSiam [9], which is not essential, but leads to a slight increase in the performance empirically.

Cluster Predictor. The cluster predictor consists of 2 self-attention layers. These attention layers consider temporal context while the module optimizes clustering prototypes.

Optimization. We apply the Adam optimizer [25] to update the model parameters. We use different batch sizes for each dataset: 32 for PennAction, 16 for H2O, and 4 for IKEA ASM. We start with a learning rate of 3×10^{-3} and decay it by a factor of 2 every 50 epochs until 150 epochs.

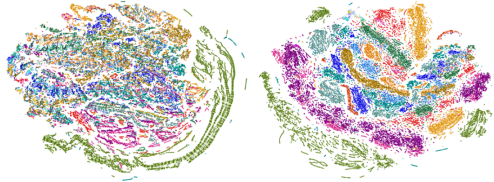


Figure 3. **t-SNE visualization of the learned embedding trained on multi activity on PennAction.** (left) CASA shows embeddings fall into a single homogeneous space, while (right) ours can learn more generalizable and discriminative representations. Each color represents each activity.

For the CASA baselines and the skeletal augmentation, we use their public code and parameters as described in [28].

4.3. Evaluation Metrics

We use the following evaluation metrics for the tasks of fine-grained video understanding. We do not use any labels for the training stage and only use them for the evaluation stage to compute the performance by training a linear classifier for the phase classification, and a linear regressor for the phase progress, as in the literature [16, 28, 42].

Phase Classification is per-frame classification. We train the model without labels, learn a linear classifier with phase labels (e.g., *bat swung back*, *bat hits ball*), and evaluate performance in the same activity.

Frame Retrieval computes the average precision (AP), which shows the success rate of retrieving the frames with the same phase label in K frames using K -nearest neighbors in the embedding space.

Phase Progress measures embedding effectiveness in capturing action progress.

Kendall’s Tau is a statistical measure of the alignment quality between two videos, which does not require any phase labels, unlike the other metrics.

Action Recognition is per-clip classification. It measures the accuracy of the actions performed. We evaluate it across the entire H2O and PennAction datasets. Unlike phase classification, which is limited by a monotonic sequence, action recognition is not bound by this restriction and can assess classification performance across multiple activities.

4.4. Fine-grained Video Understanding

We evaluate the performance of MASA in the context of fine-grained video understanding, comparing our results against state-of-the-art approaches. We report our results in two different modalities, RGB and 3D skeleton. Our method outperforms most of the metrics on both modalities.

Table 1 presents a comprehensive overview of our comparative analysis. Notably, our method consistently achieves superior performance compared to previous approaches, particularly on the PennAction dataset and the

Table 1. **Performance comparison of phase classification, video progress, and Kendall’s Tau.** The table illustrates superior performance across various datasets across most of the evaluation metrics for RGB modality. Additionally, for 3D skeletons, our proposed approach surpasses the state-of-the-art keypoints-based method.

Method	Modality	PennAction [51]					H2O [27]					IKEA ASM [3]		
		% of Labels →			Progress	τ	% of Labels →			Progress	τ	% of Labels →		
		10	50	100			10	50	100			10	50	100
LA2DS [42]	2D heatmap	89.27	92.30	92.63	0.9348	<u>0.9887</u>	<u>55.86</u>	64.58	70.12	<u>0.9280</u>	0.9670	26.43	32.56	34.73
LAV [21]	3D skeleton	79.83	80.25	80.20	0.6404	0.6983	37.05	39.50	40.45	-	-	14.52	16.31	18.63
TCC [16]	3D skeleton	79.53	83.75	84.51	0.6268	0.6267	30.40	40.20	42.72	-	-	11.95	13.53	18.63
CASA [28]	3D skeleton	88.55	91.87	92.20	<u>0.9449</u>	0.9728	43.50	62.51	68.78	0.9086	0.9465	21.32	31.52	31.06
MASA (ours)	3D skeleton	89.26	92.46	93.03	0.9342	0.9585	45.94	<u>69.97</u>	<u>75.17</u>	0.9400	<u>0.9674</u>	27.17	<u>34.55</u>	<u>36.87</u>
TCC [16]	RGB	79.72	81.11	81.35	0.6638	0.7012	43.30	52.48	52.78	-	-	27.74	25.70	26.80
TCN [37]	RGB	81.99	83.67	84.04	0.6762	0.7328	-	-	-	-	-	25.17	25.70	26.80
LAV [21]	RGB	83.56	83.95	84.25	0.6613	0.8047	35.38	51.66	53.43	0.5913	0.5323	<u>29.78</u>	29.85	30.43
VAVA [31]	RGB	83.89	84.23	84.48	-	-	-	-	-	-	-	31.66	33.79	32.91
LA2DS [42]	RGB	84.75	86.91	88.58	0.8891	0.9625	48.08	63.26	68.85	0.9113	0.9478	28.31	32.98	35.55
VSP [50]	RGB	<u>92.24</u>	<u>92.48</u>	93.12	0.9230	0.9860	-	-	-	-	-	-	-	36.09
CARL [7]	RGB	-	-	<u>93.18</u>	0.931	0.9680	-	-	-	-	-	-	-	-
MASA (ours)	RGB	92.40	92.84	93.63	0.9914	0.9894	74.71	80.35	83.68	0.9275	0.9857	24.31	35.18	38.83

H2O dataset. In the case of using 100% labels for the linear classifier, our method outperforms state-of-the-art techniques by a substantial margin, exhibiting performance gains of 0.45%, 2.74%, and 13.56% on PennAction, IKEA ASM, and H2O, respectively. Notably, our method demonstrates significant performance gain for the H2O dataset for every portion of labels (10%, 50%, 100%), which shows the effectiveness of our clip-level clustering for sequences that include multiple procedural steps to complete the pouring milk task. Importantly, even when utilizing a reduced portion (10% or 50%) of labels for training, our method remains competitive or surpasses other methodologies. This underscores the robustness and generalizability of our approach across different datasets.

As shown in Table 1, the phase progress and Kendall’s tau measure how well the sequences are aligned by phase and by mutual order. Our method achieves high scores on both metrics, thanks to the context module. In Figure 1, we present qualitative results for sequence alignment. More qualitative results will be in the supplementary material.

4.5. Generalization Capabilities

We distinguish terminologies for clarity: **Action**: a single instance, e.g., Baseball Swing. **Activity**: a series of actions that form a complete monotonic sequence. **Phase**: a state defined by **key events** that mark significant transitions within the sequence. E.g., there are 3 phases ($P_{1,2,3}$) in Baseball Swing: $P_1 \rightarrow$ Bat swung back $\rightarrow P_2 \rightarrow$ Bat hit $\rightarrow P_3$. The existing methods for achieving optimal performance are mostly limited to aligning sequences of the same activity only and require separate models to be trained for each activity. In contrast, our approach demonstrates successful generalization to multiple activities. To validate this generalizability, we conducted additional experiments using training on all activities on different tasks.

Multi Activity vs. Single Activity. We compare the performance of our approach when it is trained on all activities within the PennAction dataset, which has the highest number of sequences and activities among evaluation datasets, compared to training separate models for each individual activity. To set up baselines, we select two state-of-the-art methods for each modality, CASA [28] and CARL [7]. We retrained CASA with 3D skeletons on all activities and assessed its performance with the code that the authors provided. For the CARL baseline implementation, we also adopt the same code and parameters as specified in their paper to train a model per action. As presented in Table 2, on 3D skeleton our proposed method exhibits a performance increase almost across all the metrics, which underscores the remarkable generalizability of our approach. In the case of Multi activity, CASA shows a significant drop in performance across all metrics compared to when trained on one activity. Whereas MASA on 3D skeleton only slightly decreases for 50% and 100% phase classification while keeping other metrics increased. The performance gain is more noticeable on RGB data. While CARL performs comparably or slightly better when using individual models per action, MASA stands out by outperforming all metrics when training a single model for all the activities simultaneously. This result demonstrates the effectiveness of clustering for sequence alignment, as it prevents embedding collapse and allows the model to leverage features shared across different activities. More comparisons are in the supplementary material. Additionally, we visually compare the learned embeddings of CASA to ours when trained on multiple activities. As Figure 3 illustrates the learned embeddings fall into a single homogeneous space across different activities, which results in difficulties in identifying different activities, while the learned embeddings by our method differentiate well between different activities.

Table 2. **Comparison of our approach and CASA/CARL when trained on all activities of the PennAction dataset.** Despite a tenfold increase in the number of activities, our method demonstrates a significant performance improvement with the RGB modality and only a minor drop in performance with the 3D skeleton modality, highlighting its generalization to diverse activities.

Method	Mod.	Multi-Action	Progress	τ	Retriev.	% of Labels \rightarrow		
						10	50	100
CASA [28]	3D	\times	0.9449	0.9728	89.07	88.55	91.87	92.20
CASA [28]	3D	\checkmark	0.9012	0.9236	84.95	84.37	90.40	90.12
MASA (ours)	3D	\times	0.9341	0.9585	90.88	89.26	92.46	93.03
MASA (ours)	3D	\checkmark	0.9906	0.9652	90.96	90.16	91.71	92.23
CARL [7]	RGB	\times	0.931	0.968	91.39	-	-	93.18
CARL [7]	RGB	\checkmark	0.918	0.985	91.82	-	-	93.07
MASA (ours)	RGB	\times	0.9103	0.9646	91.56	90.43	91.25	92.12
MASA (ours)	RGB	\checkmark	0.9914	0.9894	93.07	92.40	92.84	93.63

Table 3. **Comparing our method’s performance in action recognition with RGB images, 3D hand poses, and their combination.** It demonstrates the effectiveness of our method across different modalities.

Dataset	Method	Modality	SSL	Acc. (%)
H2O [27]	Linear classifier	3D skeleton	-	33.88
	CASA	3D skeleton	\checkmark	47.52
	TA-GCN [27]	3D skeleton	\times	58.92
	Ours	3D skeleton	\checkmark	57.03
	Wen et al. [45]	RGB	\times	86.36
	Linear classifier	RGB	-	79.34
	MASA (ours)	RGB	\checkmark	81.81
	MASA (ours)	3D skeleton & RGB	\checkmark	82.64
PennAction [51]	Linear classifier	3D skeleton	-	82.36
	CASA	3D skeleton	\checkmark	90.96
	MASA (ours)	3D skeleton	\checkmark	95.80
	Linear classifier	RGB	-	91.50
	MASA (ours)	RGB	\checkmark	96.73
	MASA (ours)	3D skeleton & RGB	\checkmark	97.03

Action Recognition with Different Modalities. We evaluate the effectiveness of MASA for the task of action recognition. Action recognition also allows us to measure the performance of clustering across different activities. The purpose of this evaluation is to observe the generalization ability across various actions. For this task, we use action recognition labels from the H2O dataset and repurpose phase labels (atomic action) as action labels in the PennAction dataset to create more diverse action classifications. For the evaluation, we uniformly sample 16 frames per action and run a linear classifier with the training labels to maintain a self-supervised manner. As a baseline, we run a linear classifier using 3D hand poses and RGB images instead of learned embeddings. MASA shows better action recognition performance across two datasets and modalities compared to the linear classifier and CASA baselines.

To compare between modalities, as RGB modality compared to 3D hand skeleton modality provides a richer representation, we achieve a significant improvement of 24.78% and 0.93% in accuracy on H2O and PennAction, respectively. Furthermore, we also address multi modality for action recognition. We fuse 3D hands and RGB images together by concatenating their features before inputting them

into our context-aware module. The results presented in Table 3 highlight the effectiveness of our approach across different modalities. When combining 3D hand skeletons and RGB data, our results demonstrate great performance levels comparable to state-of-the-art supervised learning-based methods [12, 45] even though we only use a simple linear classifier to recognize actions. This shows the potential of our method in addressing general action recognition tasks.

4.6. Ablation Studies

Table 4. **Impact of component exclusions on evaluation metrics on the H2O dataset.** Each component contributes to the performance, proving our design choice.

w/o	Self att.	Stop gradient	Dual aug.	Trim aug.	Cluster predictor	Cross att.	-
Class.	74.98	76.68	77.68	78.87	79.73	79.33	83.68
Progress	0.9335	0.9173	0.9092	0.9192	0.9202	0.9226	0.9275
Tau	0.9630	0.9712	0.9803	0.9824	0.9833	0.9751	0.9857

We ablate MASA on the H2O (Pouring Milk) dataset. The results on phase classification, phase, progress, and Kendall’s Tau metrics are shown in Table 4. Our study confirms the importance of the stop gradient, the cluster predictor, and trimming for the clustering task. Notably, the exclusion of stop gradient leads to a significant drop of 7.0% in classification accuracy. The collapse of embeddings happens with the clustering predictor in this case. Moreover, omitting either of the attention modules results in a decrease in accuracy by about 4.35% and 8.7% for cross-attention and self-attention in classification, respectively. This indicates that the attention module plays an important role in learning the representations in the context-aware module.

5. Conclusion

In this paper, we present MASA, a novel framework for self-supervised sequence alignment that can handle a wide range of activities and scenarios. The proposed framework introduces clip-level implicit clustering and identification of prototypes for different activities in the latent space as an additional constraint in the optimization schema for the task of temporal video alignment. We also propose a dual augmentation technique, which can learn more generalizable and discriminative representations than existing methods. We demonstrated the superiority of MASA on three diverse datasets compared to the state-of-the-art methods and provided ablation studies and quantitative analysis. Naturally, the precision of this method may be impacted, especially for the very long videos as we showed in our experiments, which can be considered as a future work direction. Nevertheless, our approach is not limited to RGB only and can leverage other modalities such as skeletons as we demonstrated. Overall, this paper makes significant contributions to the field of temporal sequence alignment and has the potential to impact a wide range of applications.

References

- [1] Unaiza Ahsan, Chen Sun, and Irfan Essa. Discrimnet: Semi-supervised action recognition from videos using generative adversarial networks. *arXiv preprint arXiv:1801.07230*, 2018. 2
- [2] Yuki Markus Asano, Christian Rupprecht, and Andrea Vedaldi. Self-labelling via simultaneous clustering and representation learning. *arXiv preprint arXiv:1911.05371*, 2019. 2
- [3] Yizhak Ben-Shabat, Xin Yu, Fatemehsadat Saleh, Dylan Campbell, Cristian Rodriguez-Opazo, Hongdong Li, and Stephen Gould. The ikea asm dataset: Understanding people assembling furniture through actions, objects and pose. 2020. 2, 5, 7
- [4] Mathilde Caron, Ishan Misra, Julien Mairal, Priya Goyal, Piotr Bojanowski, and Armand Joulin. Unsupervised learning of visual features by contrasting cluster assignments. *Advances in neural information processing systems*, 33:9912–9924, 2020. 2
- [5] Mathilde Caron, Hugo Touvron, Ishan Misra, Hervé Jégou, Julien Mairal, Piotr Bojanowski, and Armand Joulin. Emerging properties in self-supervised vision transformers. *arXiv preprint arXiv:2104.14294*, 2021. 2
- [6] Joao Carreira and Andrew Zisserman. Quo vadis, action recognition? a new model and the kinetics dataset. In *proceedings of the IEEE Conference on Computer Vision and Pattern Recognition*, pages 6299–6308, 2017. 3
- [7] Minghao Chen, Fangyun Wei, Chong Li, and Deng Cai. Frame-wise action representations for long videos via sequence contrastive learning. In *Proceedings of the IEEE/CVF Conference on Computer Vision and Pattern Recognition*, pages 13801–13810, 2022. 1, 3, 7, 8
- [8] Ting Chen, Simon Kornblith, Mohammad Norouzi, and Geoffrey Hinton. A simple framework for contrastive learning of visual representations. In *International conference on machine learning*, pages 1597–1607. PMLR, 2020. 2, 4
- [9] Xinlei Chen and Kaiming He. Exploring simple siamese representation learning. In *Proceedings of the IEEE/CVF conference on computer vision and pattern recognition*, pages 15750–15758, 2021. 2, 5, 6
- [10] Xinlei Chen, Haoqi Fan, Ross Girshick, and Kaiming He. Improved baselines with momentum contrastive learning. *arXiv preprint arXiv:2003.04297*, 2020. 2
- [11] Ke Cheng, Yifan Zhang, Xiangyu He, Weihang Chen, Jian Cheng, and Hanqing Lu. Skeleton-based action recognition with shift graph convolutional network. In *CVPR*, 2020. 3
- [12] Hoseong Cho, Chanwoo Kim, Jihyeon Kim, Seongyeon Lee, Elkhan Ismayilzada, and Seungryul Baek. Transformer-based unified recognition of two hands manipulating objects. In *Proceedings of the IEEE/CVF Conference on Computer Vision and Pattern Recognition*, pages 4769–4778, 2023. 3, 8
- [13] Ishan Dave, Rohit Gupta, Mamshad Nayeem Rizve, and Mubarak Shah. Tclr: Temporal contrastive learning for video representation. *Computer Vision and Image Understanding*, 219:103406, 2022. 2
- [14] Ali Diba, Vivek Sharma, Luc Van Gool, and Rainer Stiefelhagen. Dynamonet: Dynamic action and motion network. In *Proceedings of the IEEE/CVF International Conference on Computer Vision*, pages 6192–6201, 2019. 2
- [15] Gerard Donahue and Ehsan Elhamifar. Learning to predict activity progress by self-supervised video alignment. In *Proceedings of the IEEE/CVF Conference on Computer Vision and Pattern Recognition*, pages 18667–18677, 2024. 3
- [16] Debidatta Dwibedi, Yusuf Aytar, Jonathan Tompson, Pierre Sermanet, and Andrew Zisserman. Temporal cycle-consistency learning. In *Proceedings of the IEEE/CVF Conference on Computer Vision and Pattern Recognition*, pages 1801–1810, 2019. 1, 3, 4, 5, 6, 7
- [17] Christoph Feichtenhofer, Haoqi Fan, Jitendra Malik, and Kaiming He. Slowfast networks for video recognition. In *Proceedings of the IEEE/CVF international conference on computer vision*, pages 6202–6211, 2019. 3
- [18] Christoph Feichtenhofer, Haoqi Fan, Bo Xiong, Ross Girshick, and Kaiming He. A large-scale study on unsupervised spatiotemporal representation learning. In *Proceedings of the IEEE/CVF Conference on Computer Vision and Pattern Recognition*, pages 3299–3309, 2021. 2
- [19] Jean-Bastien Grill, Florian Strub, Florent Altché, Corentin Tallec, Pierre Richemond, Elena Buchatskaya, Carl Doersch, Bernardo Avila Pires, Zhaohan Guo, Mohammad Gheshlaghi Azar, et al. Bootstrap your own latent—a new approach to self-supervised learning. *Advances in neural information processing systems*, 33:21271–21284, 2020. 2
- [20] Tengda Han, Weidi Xie, and Andrew Zisserman. Memory-augmented dense predictive coding for video representation learning. In *ECCV*, 2020. 3
- [21] Sanjay Haresh, Sateesh Kumar, Huseyin Coskun, Shahram N Syed, Andrey Konin, Zeeshan Zia, and Quoc-Huy Tran. Learning by aligning videos in time. In *Proceedings of the IEEE/CVF Conference on Computer Vision and Pattern Recognition*, pages 5548–5558, 2021. 1, 3, 5, 6, 7
- [22] Kaiming He, Haoqi Fan, Yuxin Wu, Saining Xie, and Ross Girshick. Momentum contrast for unsupervised visual representation learning. In *Proceedings of the IEEE/CVF Conference on Computer Vision and Pattern Recognition*, pages 9729–9738, 2020. 2
- [23] Kaiming He, Xinlei Chen, Saining Xie, Yanghao Li, Piotr Dollár, and Ross Girshick. Masked autoencoders are scalable vision learners. In *Proceedings of the IEEE/CVF conference on computer vision and pattern recognition*, pages 16000–16009, 2022. 2
- [24] Kai Hu, Jie Shao, Yuan Liu, Bhiksha Raj, Marios Savvides, and Zhiqiang Shen. Contrast and order representations for video self-supervised learning. In *Proceedings of the IEEE/CVF International Conference on Computer Vision*, pages 7939–7949, 2021. 2
- [25] Diederik P Kingma and Jimmy Ba. Adam: A method for stochastic optimization. *arXiv preprint arXiv:1412.6980*, 2014. 6
- [26] Sateesh Kumar, Sanjay Haresh, Awais Ahmed, Andrey Konin, M Zeeshan Zia, and Quoc-Huy Tran. Unsupervised action segmentation by joint representation learning and on-line clustering. In *Proceedings of the IEEE/CVF Conference*

- on *Computer Vision and Pattern Recognition*, pages 20174–20185, 2022. 3
- [27] Taein Kwon, Bugra Tekin, Jan Stühmer, Federica Bogo, and Marc Pollefeys. H2o: Two hands manipulating objects for first person interaction recognition. In *Proceedings of the IEEE/CVF International Conference on Computer Vision (ICCV)*, pages 10138–10148, 2021. 2, 5, 7, 8
- [28] Taein Kwon, Bugra Tekin, Siyu Tang, and Marc Pollefeys. Context-aware sequence alignment using 4d skeletal augmentation. In *Proceedings of the IEEE/CVF Conference on Computer Vision and Pattern Recognition*, pages 8172–8182, 2022. 1, 2, 3, 4, 5, 6, 7, 8
- [29] Maosen Li, Siheng Chen, Xu Chen, Ya Zhang, Yanfeng Wang, and Qi Tian. Actional-structural graph convolutional networks for skeleton-based action recognition. In *Proceedings of the IEEE/CVF conference on computer vision and pattern recognition*, pages 3595–3603, 2019. 3
- [30] Junan Lin, Zhichao Sun, Enjie Cao, Taein Kwon, Mahdi Rad, and Marc Pollefeys. Casar: Contact-aware skeletal action recognition. *arXiv preprint arXiv:2309.10001*, 2023. 3
- [31] Weizhe Liu, Bugra Tekin, Huseyin Coskun, Vibhav Vineet, Pascal Fua, and Marc Pollefeys. Learning to align sequential actions in the wild. In *Proceedings of the IEEE/CVF Conference on Computer Vision and Pattern Recognition*, pages 2181–2191, 2022. 3, 5, 6, 7
- [32] Ziyu Liu, Hongwen Zhang, Zhenghao Chen, Zhiyong Wang, and Wanli Ouyang. Disentangling and unifying graph convolutions for skeleton-based action recognition. In *CVPR*, 2020. 3
- [33] Yunyao Mao, Jiajun Deng, Wengang Zhou, Yao Fang, Wanli Ouyang, and Houqiang Li. Masked motion predictors are strong 3d action representation learners. In *Proceedings of the IEEE/CVF International Conference on Computer Vision*, pages 10181–10191, 2023. 3
- [34] Maxime Oquab, Timothée Darcet, Théo Moutakanni, Huy Vo, Marc Szafraniec, Vasil Khalidov, Pierre Fernandez, Daniel Haziza, Francisco Massa, Alaaeldin El-Nouby, et al. DINOv2: Learning robust visual features without supervision. *arXiv preprint arXiv:2304.07193*, 2023. 3, 4, 6
- [35] Rui Qian, Tianjian Meng, Boqing Gong, Ming-Hsuan Yang, Huisheng Wang, Serge Belongie, and Yin Cui. Spatiotemporal contrastive video representation learning. In *Proceedings of the IEEE/CVF Conference on Computer Vision and Pattern Recognition*, pages 6964–6974, 2021. 2, 3
- [36] Yu Rong, Takaaki Shiratori, and Hanbyul Joo. Frankmocap: A monocular 3d whole-body pose estimation system via regression and integration. In *IEEE International Conference on Computer Vision Workshops*, 2021. 4, 6
- [37] Pierre Sermanet, Corey Lynch, Yevgen Chebotar, Jasmine Hsu, Eric Jang, Stefan Schaal, Sergey Levine, and Google Brain. Time-contrastive networks: Self-supervised learning from video. In *2018 IEEE international conference on robotics and automation (ICRA)*, pages 1134–1141. IEEE, 2018. 1, 2, 7
- [38] Lei Shi, Yifan Zhang, Jian Cheng, and Hanqing Lu. Two-stream adaptive graph convolutional networks for skeleton-based action recognition. In *CVPR*, 2019. 3
- [39] Kun Su, Xiulong Liu, and Eli Shlizerman. Predict & cluster: Unsupervised skeleton based action recognition. In *Proceedings of the IEEE/CVF Conference on Computer Vision and Pattern Recognition*, pages 9631–9640, 2020. 3
- [40] Yukun Su, Guosheng Lin, and Qingyao Wu. Self-supervised 3d skeleton action representation learning with motion consistency and continuity. In *Proceedings of the IEEE/CVF International Conference on Computer Vision*, pages 13328–13338, 2021. 3
- [41] Zhan Tong, Yibing Song, Jue Wang, and Limin Wang. Videomae: Masked autoencoders are data-efficient learners for self-supervised video pre-training. *Advances in neural information processing systems*, 35:10078–10093, 2022. 2, 3
- [42] Quoc-Huy Tran, Muhammad Ahmed, Ahmed Mehmood, M Hassan Ahmed, Murad Popattia, Andrey Konin, and M Zeeshan Zia. Learning by aligning 2d skeleton sequences in time. *arXiv preprint arXiv:2305.19480*, 2023. 1, 2, 3, 4, 5, 6, 7
- [43] Ashish Vaswani, Noam Shazeer, Niki Parmar, Jakob Uszkoreit, Llion Jones, Aidan N Gomez, Lukasz Kaiser, and Illia Polosukhin. Attention is all you need. In *Advances in neural information processing systems*, pages 5998–6008, 2017. 4
- [44] Limin Wang, Bingkun Huang, Zhiyu Zhao, Zhan Tong, Yinan He, Yi Wang, Yali Wang, and Yu Qiao. Videomae v2: Scaling video masked autoencoders with dual masking. In *Proceedings of the IEEE/CVF Conference on Computer Vision and Pattern Recognition*, pages 14549–14560, 2023. 2, 3
- [45] Yilin Wen, Hao Pan, Lei Yang, Jia Pan, Taku Komura, and Wenping Wang. Hierarchical temporal transformer for 3d hand pose estimation and action recognition from egocentric rgb videos. In *Proceedings of the IEEE/CVF Conference on Computer Vision and Pattern Recognition*, pages 21243–21253, 2023. 3, 8
- [46] Zhirong Wu, Yuanjun Xiong, Stella X Yu, and Dahua Lin. Unsupervised feature learning via non-parametric instance discrimination. In *Proceedings of the IEEE conference on computer vision and pattern recognition*, pages 3733–3742, 2018. 2
- [47] Hong Yan, Yang Liu, Yushen Wei, Zhen Li, Guanbin Li, and Liang Lin. Skeletonmae: graph-based masked autoencoder for skeleton sequence pre-training. In *Proceedings of the IEEE/CVF International Conference on Computer Vision*, pages 5606–5618, 2023. 3
- [48] Sijie Yan, Yuanjun Xiong, and Dahua Lin. Spatial temporal graph convolutional networks for skeleton-based action recognition. In *Thirty-second AAAI conference on artificial intelligence*, 2018. 3
- [49] Hang Zhang, Xin Li, and Lidong Bing. Video-llama: An instruction-tuned audio-visual language model for video understanding. *arXiv preprint arXiv:2306.02858*, 2023. 3
- [50] Heng Zhang, Daqing Liu, Qi Zheng, and Bing Su. Modeling video as stochastic processes for fine-grained video representation learning. In *Proceedings of the IEEE/CVF Conference on Computer Vision and Pattern Recognition*, pages 2225–2234, 2023. 3, 7

- [51] Weiyu Zhang, Menglong Zhu, and Konstantinos G. Derpanis. From actemes to action: A strongly-supervised representation for detailed action understanding. In *Proceedings of the IEEE International Conference on Computer Vision (ICCV)*, 2013. [2](#), [5](#), [7](#), [8](#)

Multi Activity Sequence Alignment via Implicit Clustering

Taein Kwon¹

Zador Pataki¹

Mahdi Rad²

Marc Pollefeys^{1,2}

¹ETH Zürich ²Microsoft MR & AI Lab, Zürich

In this supplementary material, we first elaborate on our implementation details, such as the parameter, augmentation, image backbone, and pose estimator settings. We then demonstrate the results on the task of frame retrieval to show the success rate of retrieving the frames with the same phase label. Furthermore, we present qualitative results using confusion matrices to have a better understanding of action recognition capabilities through our method. Finally, we show more qualitative results, including frame retrieval and sequence alignment on both RGB and 3D skeleton modalities.

S.1. Implementation Details

Parameter Settings.

Hyperparameter	Value		
Optimizer	ADAM		
Temperature (λ_{temp})	0.1		
3D geometric noise probability	30 %		
Noise standard deviation (σ)	10° (angle), 0.1 (VPoser, translation)		
Number of attention layers (N_{att})	4		
Datasets	Penn	H2O	IKEA
Batch Size	64	32	16
Input dimension	75	51	75
Number of heads (parallel attention layers)	15	17	15
Learning rate	3×10^{-3}	1.5×10^{-3}	7.5×10^{-4}
Learning rate (all)	3×10^{-4}	1.5×10^{-4}	-

Table S1. Hyperparameters in our experiment.

In Table S1, we list hyperparameters that we use for training our models. We will also release our code upon acceptance of the paper.

Augmentations. In accordance with the methodology proposed by CASA [7], we employ spatial augmentations to enhance the robustness of our model. Specifically, we utilize four spatial augmentations (angle, flip, translation, and VPoser) for the PennAction and IKEA ASM datasets and three spatial augmentations (angle, flip, and translation) for the H2O dataset. The noise parameters associated with these augmentations are detailed in Table S1. Notably, our method diverges from CASA in terms of temporal augmentations. Unlike CASA, our approach contains a temporal cropping method that helps to learn partially trimmed sequence clustering and our proposed Dual Augmentation technique, which can cover slower augmentation.

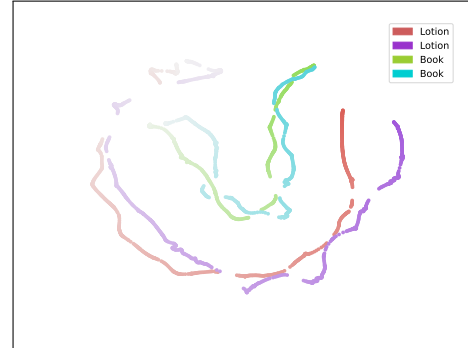


Figure S1. The t-SNE visualization of different activities in the H2O dataset. Blue and green are book activity sequences while red and violet are lotions sequences. Intra-class sequences of books and lotions exhibit strong alignment, whereas inter-class separation is pronounced in the embedding space. Less opacity means early in the sequence.

Image Backbone Settings. For this image backbone, we use the pretrained DINO [10] model. DINO is a vision transformer-based model, trained using a self-supervised learning method on 142 million unlabeled images. We used a distilled version of the original model, which generates visual features with a dimensionality of 1536.

Pose Estimator Settings. We use 3D human body pose from SMPL [11] and hand pose from MANO [12] by following CASA [7]. Both SMPL and MANO models take pose parameters $\theta_{smpl} \in \mathbb{R}^{72}$, $\theta_{mano} \in \mathbb{R}^{51 \times 2}$ and shape parameters $\beta_{smpl} \in \mathbb{R}^{10}$, $\beta_{mano} \in \mathbb{R}^{10 \times 2}$ and return 3D keypoints for body $s_{penn} \in \mathbb{R}^{25 \times 3}$ and hand $s_{hand} \in \mathbb{R}^{42 \times 3}$.

S.2. Action Recognition Qualitative Results

We illustrate the action recognition confusion matrices pertaining to the H2O dataset in Figure S2 and Figure S3. Figure S2 demonstrates the confusion matrix generated solely from hand pose inputs on the H2O dataset. Our method, based on 3D skeletal information, engages in action recognition by exploiting hand poses. However, it is noteworthy that relying exclusively on hand pose information presents a challenge in distinguishing between nouns, such

Table S2. **Comparison of frame retrieval performance.** Our framework outperforms other methods on the H2O and PennAction datasets for frame retrieval.

Datasets	Method	Modality	AP@5	AP@10	AP@15
PennAction [16]	SAL [9]	RGB	76.04	75.77	75.61
	TCN [13]	RGB	77.84	77.51	77.28
	TCC [4]	RGB	76.74	76.27	75.88
	LAV [5]	RGB	79.13	78.98	78.90
	VAVA [8]	RGB	81.52	80.47	80.67
	LA2DS [14]	2D heatmap	93.07	91.84	91.35
	CASA [7]	3D skeleton	89.90	89.44	89.07
	CARL [2]	RGB	92.28	<u>92.10</u>	<u>91.82</u>
	VSP [15]	RGB	92.56	-	-
	MASA (ours)	3D skeleton	91.19	91.03	90.88
MASA (ours)	RGB	93.01	92.91	92.82	
IKEA ASM [1]	SaL [9]	RGB	15.15	14.90	14.72
	TCN [13]	RGB	19.15	19.19	19.33
	TCC [4]	RGB	19.80	19.64	19.68
	LAV [5]	RGB	23.89	23.65	23.56
	VAVA [8]	RGB	29.58	28.74	28.48
	LA2DS [14]	2D heatmap	32.44	31.89	31.56
	CASA [7]	3D skeleton	28.92	<u>28.88</u>	<u>28.61</u>
	VSP [15]	RGB	26.54	-	-
	MASA (ours)	3D skeleton	25.44	24.57	24.55
	MASA (ours)	RGB	23.77	24.07	24.28
H2O [6]	LAV [5]	RGB	47.55	45.56	44.61
	LA2DS [14]	2D heatmap	67.51	63.11	61.75
	CASA [7]	3D skeleton	60.13	59.44	59.01
	MASA (ours)	3D skeleton	<u>66.79</u>	<u>66.18</u>	<u>66.30</u>
	MASA (ours)	RGB	78.92	78.55	78.22

Table S3. More results for multi activity training on PennAction. Most of the methods show significant performance drops when training multiple activities on one model (see Tab. 1).

Method	SAL [9]	GTCC [3]	TCC [4]	TCN [13]	LAV [5]	VAVA [8]	CARL [2]	MASA (ours)	
Single act.	Phase Class.	79.96	81.30	81.35	84.04	84.25	84.48	93.18	92.12
	Progress	0.5943	0.7080	0.6638	0.6762	0.6613	0.7090	0.9310	0.9103
	τ	0.6336	0.7012	0.8830	0.7328	0.8047	0.8050	0.9680	0.9646
Multi act.	Phase Class.	68.15	86.70	74.39	68.09	78.68	80.30	95.07	93.63
	Progress	0.3903	0.8550	0.5914	0.3834	0.6252	0.6480	0.9180	0.9894
	τ	0.4744	0.9490	0.6408	0.5417	0.6835	0.7620	0.9850	0.9914

as Lotion and Spray.

To address this challenge, we incorporate both hand poses and RGB images, as depicted in Table 4 of the main paper. Figure S3 shows the network’s enhanced ability to classify actions with the inclusion of additional texture information. This outcome indicates the efficacy of the frame alignment pretext task through multi-modal self-supervised learning for the task of action recognition.

S.3. Frame Retrieval

We present the frame retrieval performance in Table S2. Our method demonstrates strong performance on the PennAction and H2O datasets. On the IKEA ASM dataset, however, our fine-grained retrieval results show a lower level of efficacy due to the complexity of optimization in the long and non-monotonic sequences for frame retrieval. However, as shown in Table 1, MASA outperforms others in phase classification, highlighting the strong potential of our representations. Also, LA2DS has a higher dimensionality in the skeleton modality than CASA and MASA. We present the frame retrieval qualitative results in Figure S4.

S.4. Multi Activity Comparisons

Table S3 together with extensive experiments presented in our main paper supports the effectiveness of our method. The methods other than GTCC drop the phase classification performance significantly (7.43%) when trained on multiple activities. GTCC and MASA are exceptions, showing improved performance under multi activity settings. However, GTCC does not achieve optimal performance relative to MASA (by 6.93%) compared to the other baseline methods. Please note that most of the methods in the table also require action labels to train unlike MASA, which learns the representation purely without any labels.

S.5. Potential Societal Impact

While our research contributes significantly to the advancement of AR, VR, and video understanding applications, it has the potential for misuse in the surveillance and monitoring of people. Such misuse raises valid privacy concerns and should be guided by ethical AI principles.

S.6. Responsibility to Human Subjects Data

Based on our current understanding, the IKEA ASM and H2O datasets are collected in a controlled lab environment, involving carefully selected subjects. Additionally, we received confirmation from the authors of the H2O dataset that they followed proper procedures during data collection, including obtaining agreements from subjects and securing IRB approval. The PennAction dataset comprises publicly available online resources such as content from YouTube. Therefore, to the best of our knowledge, using the datasets does not contravene privacy regulations.

S.7. Qualitative Results

Figure S5 and S6 show framewise sequence alignment qualitative results compared to CASA [7] using 3D skeleton modality. To demonstrate our generalization ability with multiple activities, we use models trained on all the activities in the PennAction and H2O datasets, respectively, for visualization. MASA is able to align frames in different sequences more accurately with the multi activity training setting. Figure S7 shows alignment results using RGB modality. The results demonstrate a strong alignment performance of MASA with the high dimensional data such as RGB images.

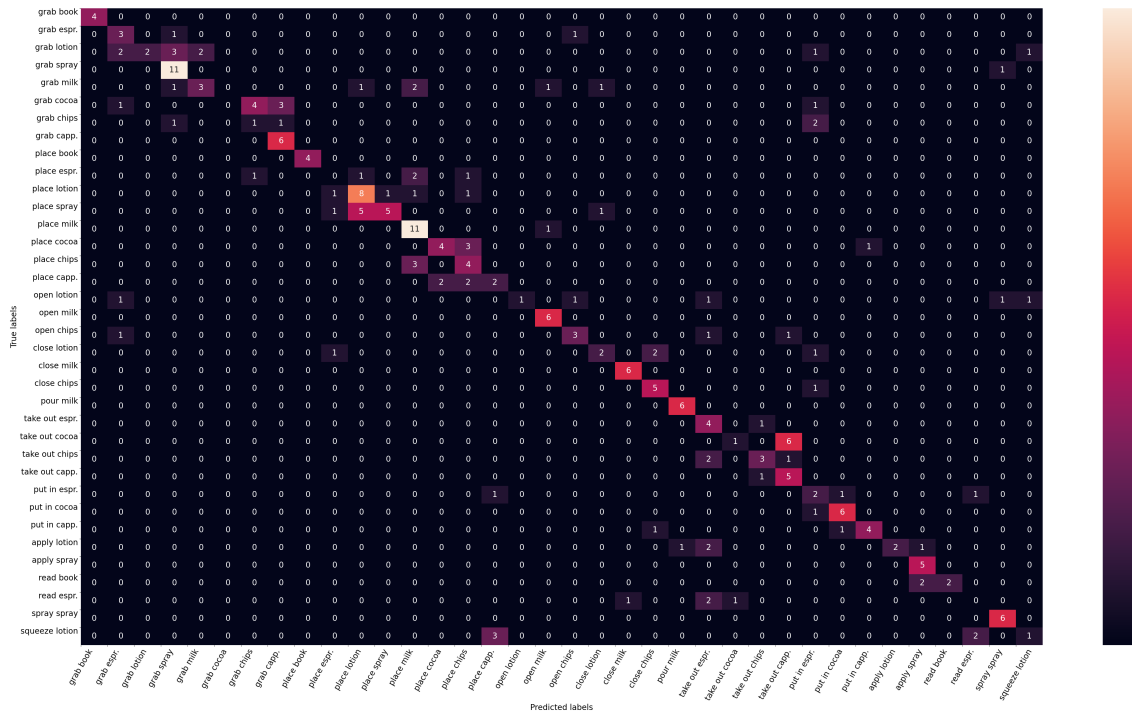


Figure S2. Action Recognition only with hand poses on the H2O dataset. The confusion matrix shows MASA successfully classifies action labels. However, the lack of texture with hand pose only leads to suboptimal performance in classifying nouns.

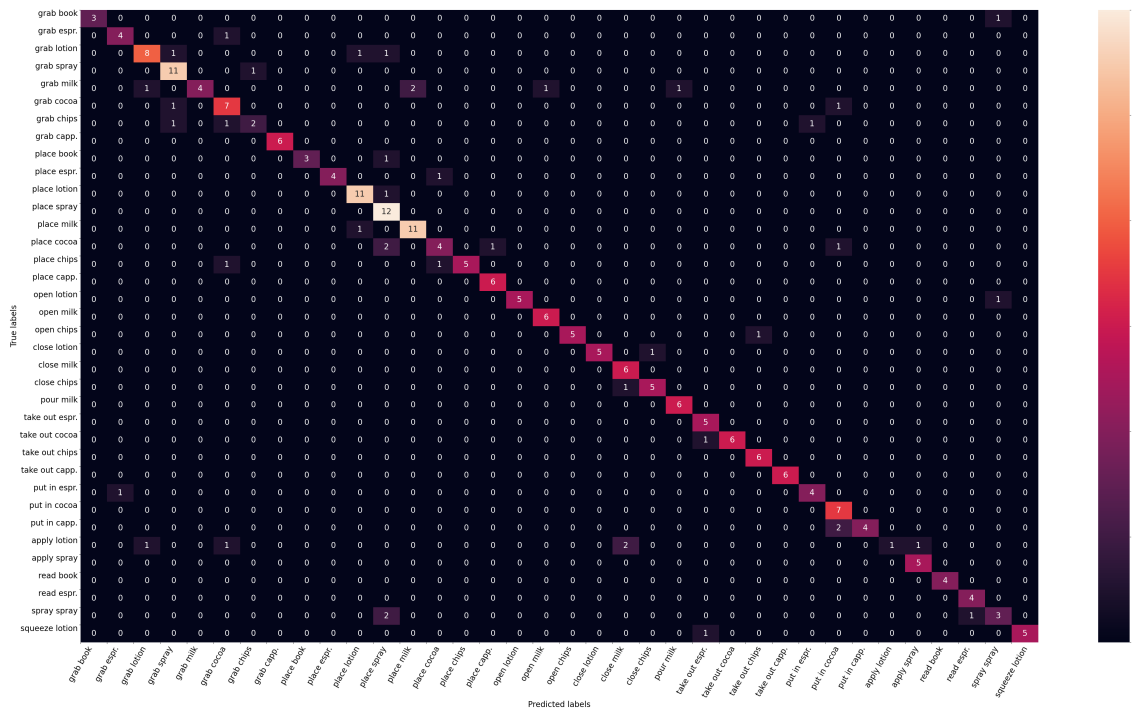
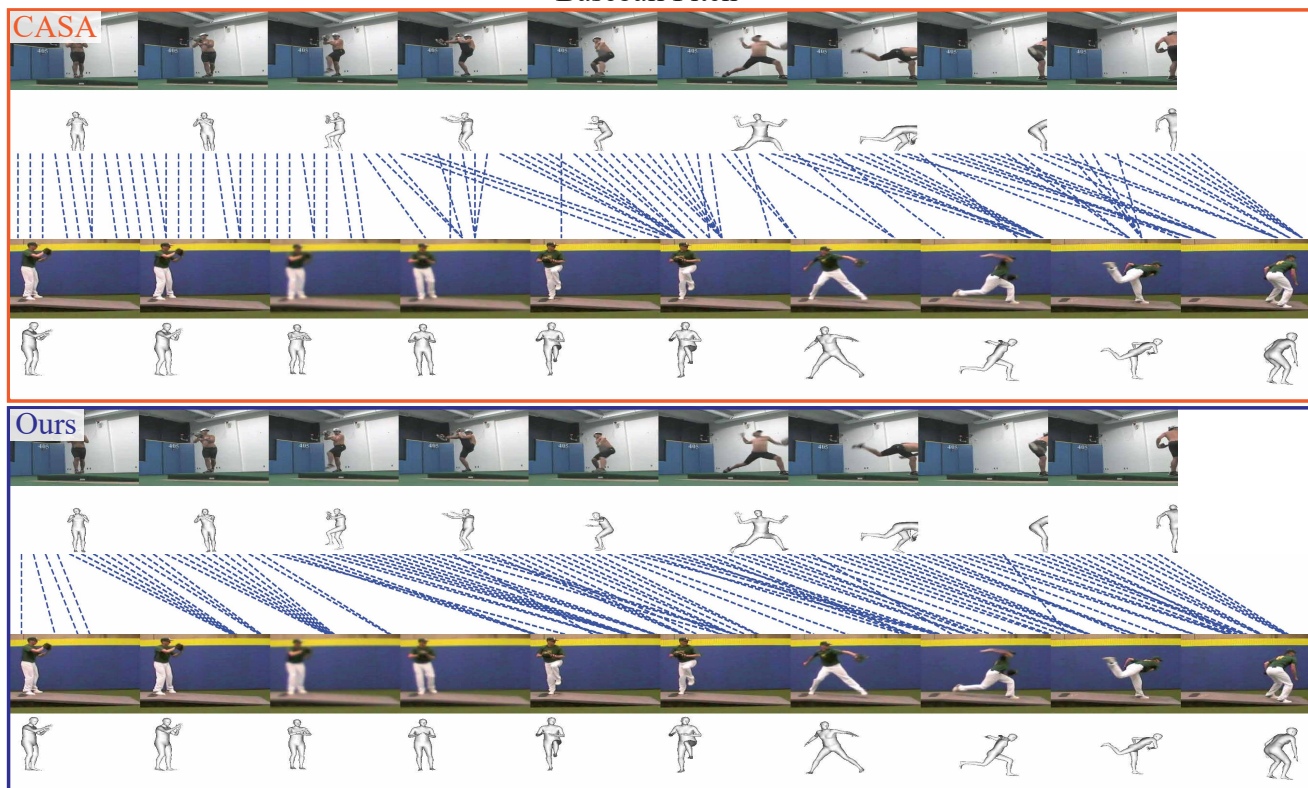


Figure S3. Action Recognition with hand poses and RGB images on the H2O dataset. Together with hand poses and RGB images, MASA achieves high performance across all actions. It shows the adaptability of our proposed framework to multimodal data.



Figure S4. **Frame retrieval results.** We present the frame retrieval results using different modalities: pose only, image only and both pose and image together (from top to bottom). The frames that are incorrectly retrieved are marked with red dashed lines. MASA retrieves more successfully when it fuses different modalities, as they complement each other. These frame retrieval results demonstrate the ability of MASA to generalize to different modalities and show its potential for multi-modal sequence alignment.

Baseball Pitch



Bowling

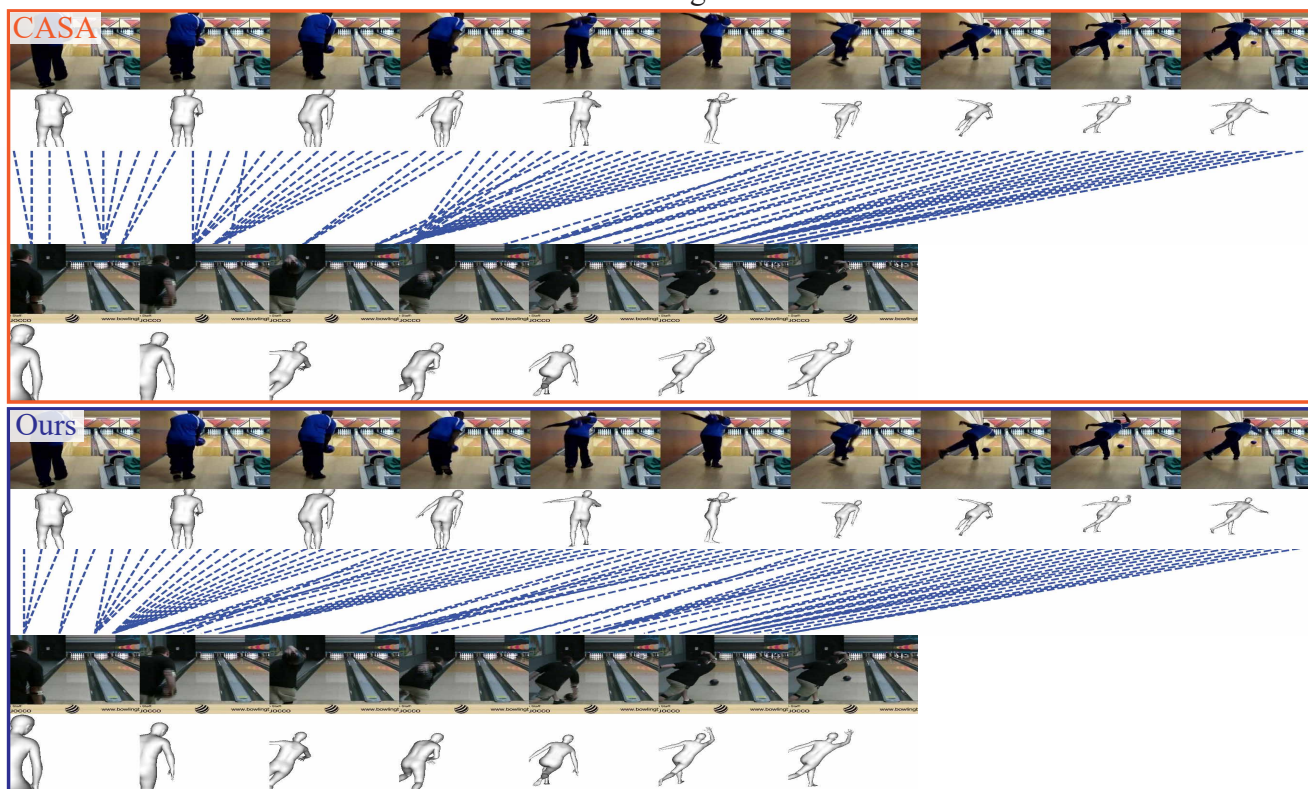
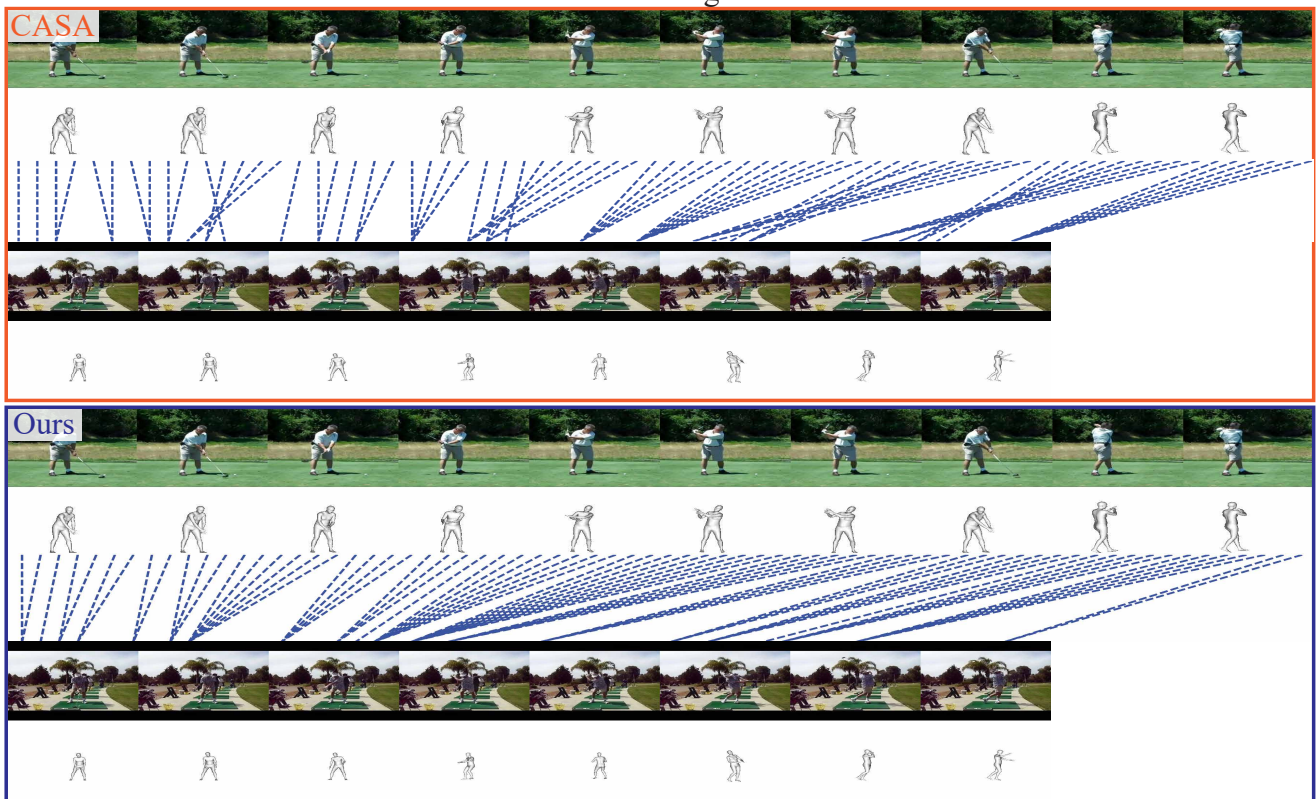


Figure S5. **Sequence alignment results.** MASA shows better alignment compared to the CASA method. For instance, in the baseball pitch example, we can observe more invalid matches that violate temporal consistency, whereas our method is more temporally consistent.

Golf Swing



Pouring Milk

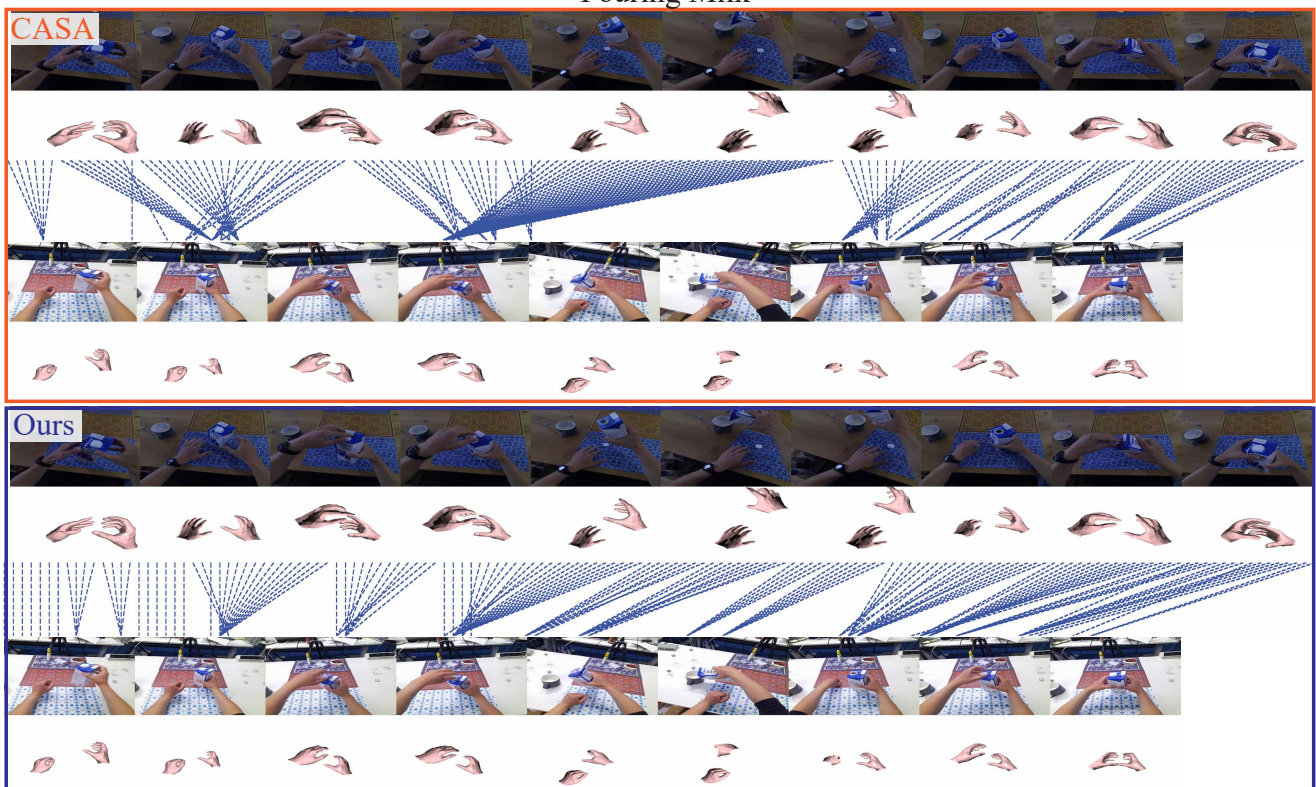
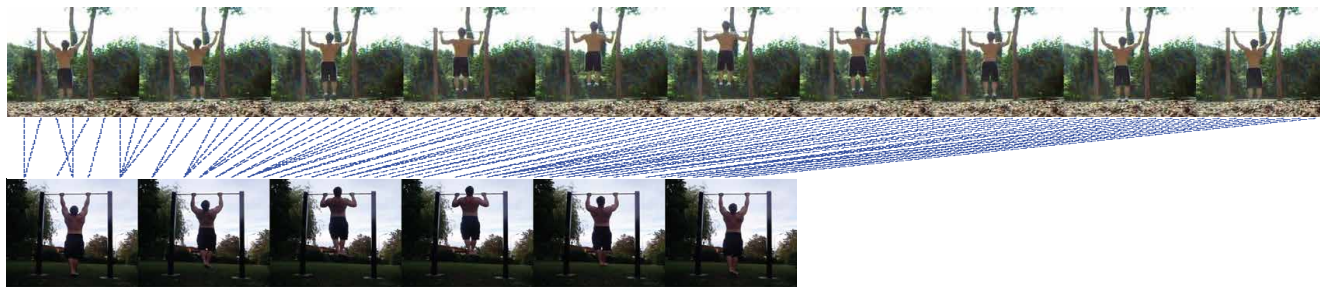
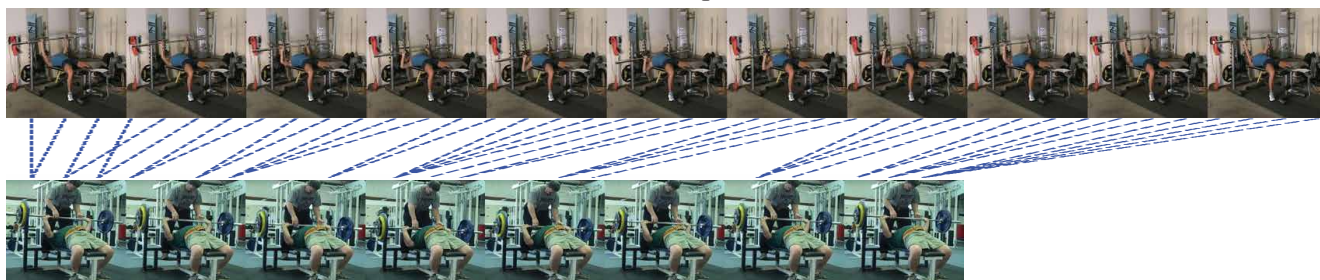


Figure S6. **Sequence alignment results.** Even in longer sequences on the H2O dataset compared to the PennAction dataset, MASA achieves robust results in alignment.

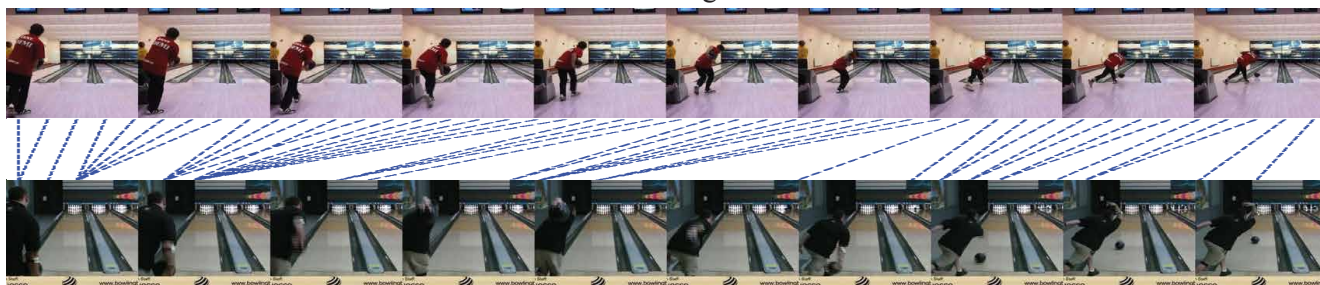
Pull Up



Push Up



Bowling



Clean And Jerk



Baseball Swing

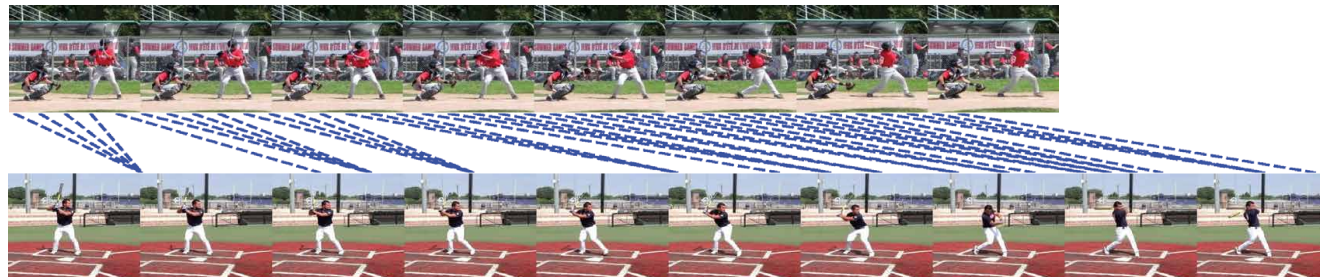


Figure S7. Sequence alignment results. MASA with RGB modality shows strong and robust results for the sequence alignment task.

References

- [1] Yizhak Ben-Shabat, Xin Yu, Fatemehsadat Saleh, Dylan Campbell, Cristian Rodriguez-Opazo, Hongdong Li, and Stephen Gould. The ikea asm dataset: Understanding people assembling furniture through actions, objects and pose. 2020. [2](#)
- [2] Minghao Chen, Fangyun Wei, Chong Li, and Deng Cai. Frame-wise action representations for long videos via sequence contrastive learning. In *Proceedings of the IEEE/CVF Conference on Computer Vision and Pattern Recognition*, pages 13801–13810, 2022. [2](#)
- [3] Gerard Donahue and Ehsan Elhamifar. Learning to predict activity progress by self-supervised video alignment. In *Proceedings of the IEEE/CVF Conference on Computer Vision and Pattern Recognition*, pages 18667–18677, 2024. [2](#)
- [4] Debidatta Dwibedi, Yusuf Aytar, Jonathan Tompson, Pierre Sermanet, and Andrew Zisserman. Temporal cycle-consistency learning. In *Proceedings of the IEEE/CVF Conference on Computer Vision and Pattern Recognition*, pages 1801–1810, 2019. [2](#)
- [5] Sanjay Haresh, Sateesh Kumar, Huseyin Coskun, Shahram N Syed, Andrey Konin, Zeeshan Zia, and Quoc-Huy Tran. Learning by aligning videos in time. In *Proceedings of the IEEE/CVF Conference on Computer Vision and Pattern Recognition*, pages 5548–5558, 2021. [2](#)
- [6] Taein Kwon, Bugra Tekin, Jan Stühmer, Federica Bogo, and Marc Pollefeys. H2o: Two hands manipulating objects for first person interaction recognition. In *Proceedings of the IEEE/CVF International Conference on Computer Vision (ICCV)*, pages 10138–10148, 2021. [2](#)
- [7] Taein Kwon, Bugra Tekin, Siyu Tang, and Marc Pollefeys. Context-aware sequence alignment using 4d skeletal augmentation. In *Proceedings of the IEEE/CVF Conference on Computer Vision and Pattern Recognition*, pages 8172–8182, 2022. [1](#), [2](#)
- [8] Weizhe Liu, Bugra Tekin, Huseyin Coskun, Vibhav Vineet, Pascal Fua, and Marc Pollefeys. Learning to align sequential actions in the wild. In *Proceedings of the IEEE/CVF Conference on Computer Vision and Pattern Recognition*, pages 2181–2191, 2022. [2](#)
- [9] Ishan Misra, C Lawrence Zitnick, and Martial Hebert. Shuffle and learn: unsupervised learning using temporal order verification. In *European Conference on Computer Vision*, pages 527–544. Springer, 2016. [2](#)
- [10] Maxime Oquab, Timothée Darcet, Théo Moutakanni, Huy Vo, Marc Szafraniec, Vasil Khalidov, Pierre Fernandez, Daniel Haziza, Francisco Massa, Alaaeldin El-Nouby, et al. Dinov2: Learning robust visual features without supervision. *arXiv preprint arXiv:2304.07193*, 2023. [1](#)
- [11] Georgios Pavlakos, Vasileios Choutas, Nima Ghorbani, Timo Bolkart, Ahmed A. A. Osman, Dimitrios Tzionas, and Michael J. Black. Expressive body capture: 3d hands, face, and body from a single image. In *Proceedings IEEE Conf. on Computer Vision and Pattern Recognition (CVPR)*, 2019. [1](#)
- [12] Javier Romero, Dimitrios Tzionas, and Michael J. Black. Embodied hands: Modeling and capturing hands and bodies together. *ACM Transactions on Graphics, (Proc. SIGGRAPH Asia)*, 36(6), 2017. [1](#)
- [13] Pierre Sermanet, Corey Lynch, Yevgen Chebotar, Jasmine Hsu, Eric Jang, Stefan Schaal, Sergey Levine, and Google Brain. Time-contrastive networks: Self-supervised learning from video. In *2018 IEEE international conference on robotics and automation (ICRA)*, pages 1134–1141. IEEE, 2018. [2](#)
- [14] Quoc-Huy Tran, Muhammad Ahmed, Ahmed Mehmood, M Hassan Ahmed, Murad Popattia, Andrey Konin, and M Zeeshan Zia. Learning by aligning 2d skeleton sequences in time. *arXiv preprint arXiv:2305.19480*, 2023. [2](#)
- [15] Heng Zhang, Daqing Liu, Qi Zheng, and Bing Su. Modeling video as stochastic processes for fine-grained video representation learning. In *Proceedings of the IEEE/CVF Conference on Computer Vision and Pattern Recognition*, pages 2225–2234, 2023. [2](#)
- [16] Weiyu Zhang, Menglong Zhu, and Konstantinos G. Derpanis. From actemes to action: A strongly-supervised representation for detailed action understanding. In *Proceedings of the IEEE International Conference on Computer Vision (ICCV)*, 2013. [2](#)